

## Article

# Direct Reduction in Greenhouse Gases by Continuous Dry (CO<sub>2</sub>) Reforming of Methane over Ni-Containing SHS Catalysts

Galina Xanthopoulou <sup>1</sup>, Savvas Varitis <sup>1,2</sup>, Manap Khan Zhumabek <sup>3,4</sup>, Konstantinos Karanasios <sup>1</sup>, George Vekinis <sup>1</sup>, Svetlana A. Tungatarova <sup>3,5,\*</sup> and Tolkyn S. Baizhumanova <sup>3,5</sup>

- <sup>1</sup> Institute of Nanoscience and Nanotechnology, NCSR Demokritos, 15310 Athens, Greece; g.xanthopoulou@inn.demokritos.gr (G.X.); s.varitis@inn.demokritos.gr (S.V.); k.karanasios@inn.demokritos.gr (K.K.); g.vekinis@inn.demokritos.gr (G.V.)
- <sup>2</sup> Department of Physics, Aristotle University of Thessaloniki, 54124 Thessaloniki, Greece
- <sup>3</sup> D.V. Sokolsky Institute of Fuel, Catalysis and Electrochemistry, 142, Kunaev Str., Almaty 050010, Kazakhstan; manapkhan\_86@mail.ru (M.Z.); baizhuma@mail.ru (T.S.B.)
- <sup>4</sup> Institute of Chemical and Biological Technologies, Satbayev University, 22a, Satpaev Str., Almaty 050013, Kazakhstan
- <sup>5</sup> Faculty of Chemistry and Chemical Technology, Al-Farabi Kazakh National University, 71, Al-Farabi Str., Almaty 050040, Kazakhstan
- \* Correspondence: tungatarova58@mail.ru; Tel.: +7-727-291-6632



**Citation:** Xanthopoulou, G.; Varitis, S.; Zhumabek, M.; Karanasios, K.; Vekinis, G.; Tungatarova, S.A.; Baizhumanova, T.S. Direct Reduction in Greenhouse Gases by Continuous Dry (CO<sub>2</sub>) Reforming of Methane over Ni-Containing SHS Catalysts. *Energies* **2021**, *14*, 6078. <https://doi.org/10.3390/en14196078>

Academic Editors: Viviana Cigolotti and Angelo Basile

Received: 24 August 2021

Accepted: 18 September 2021

Published: 24 September 2021

**Publisher's Note:** MDPI stays neutral with regard to jurisdictional claims in published maps and institutional affiliations.



**Copyright:** © 2021 by the authors. Licensee MDPI, Basel, Switzerland. This article is an open access article distributed under the terms and conditions of the Creative Commons Attribution (CC BY) license (<https://creativecommons.org/licenses/by/4.0/>).

**Abstract:** The world of energy is on the cusp of profound transformation. Hydrogen or hydrogen-containing fuel mixtures in the form of synthesis gas, as carriers of clean energy, will be in the short term among the most efficient solutions to pressing environmental problems, reducing the amount of greenhouse gases as well as pollution of cities and dependence on oil-based fuels. Carbon dioxide conversion of methane is the most promising method for the production of synthesis gas due to the simultaneous consumption of two greenhouse gases and, accordingly, a successful solution to environmental problems. Ni/Mn-based catalysts have been prepared by self-propagating high-temperature synthesis (SHS) for this process. The samples were characterized by X-ray diffraction, scanning electron microscopy, and nitrogen porosimetry. The effects of the catalysts' composition on activity, selectivity, and product yield were investigated. The influence of the content of Ni, Mn on the behavior of catalysts has been established. Comparison of spinels with different component ratios showed that they have a defective structure. Non-stoichiometric spinels with highly defective catalyst structures were obtained due to very high heating and cooling rates during SHS. They work as active sites, which underlies the high activity of the catalysts.

**Keywords:** biogas; synthesis gas; hydrogen; reforming

## 1. Introduction

The catalytic reforming of methane with carbon dioxide  $\text{CH}_4 + \text{CO}_2 \rightarrow 2\text{CO} + 2\text{H}_2$  has attracted increasing interest as an alternative for the production of hydrogen-containing fuel mixtures and synthesis gas over the past two decades. This process is industrially attractive. The International Energy Agency (IEA) World energy outlook clearly states that “natural gas is certainly set to play a central role in meeting the world’s energy needs for at least the next two-and-a-half decades” [1]. This means that technologies based on methane will have priority. However, the future of power engineering is associated, of course, with hydrogen produced in various ways. These are “gray” technologies for the production of hydrogen, which involve the emission of greenhouse gases into the atmosphere. It is blue hydrogen that is produced from natural gas. It is also an alternative technology for the production of green hydrogen through the decomposition of water using the energy of the sun. This is the most expensive hydrogen. Since 1750, the amount of methane has doubled and may double again by 2050. Each year, 350–500 million tons of CH<sub>4</sub> is added to the air through livestock farming, coal mining, oil and natural gas extraction, rice

cultivation, and landfill disposal [2]. The contribution of CO<sub>2</sub> to global annual emissions of anthropogenic greenhouse gases is about 75%, and CH<sub>4</sub> is about 14% [3]. Methane is a greenhouse gas that is more than 25 times more efficient at trapping heat in the atmosphere than carbon dioxide [4]. Reducing the sources of emissions of CH<sub>4</sub> and other greenhouse gases can lead to a decrease in the rate of global warming, reducing the risk of abrupt climate change. Many researchers have reported that Fe-, Co-, and Ni-based catalysts are highly active. However, the deactivation of catalysts is one of the main problems that arise in this process, mainly due to the deposition of carbon. Nickel catalysts have been extensively studied in the past decades, where the CH<sub>4</sub> conversion reached 68% at 80–90% selectivity to H<sub>2</sub> [5–14]. But insufficient research has been done on Co [15–17], Ni-Co [18–22], and Mn catalysts [23], for which the H<sub>2</sub> selectivity was in the region of 50%. The catalysts described in those works show high activity and excellent anti-carbon deposition properties even without prior reduction. MnO<sub>x</sub> has multiple valence states and fluorite structures with excellent oxidation and reduction characteristics [23]. It can be assumed that the Mn-doped Ni-Al-Mg-O catalyst can provide good catalytic performance in the dry reforming of methane with carbon dioxide to hydrogen and carbon monoxide.

Self-propagating high-temperature synthesis (SHS) occurs within minutes as a result of low-temperature initiation, which can lead to a high-temperature reaction. Unique materials were developed by controlled high-temperature combustion as a result of synthesis by SHS [24]. The SHS method offers a unique method for the preparation of modern, highly active ceramic catalysts, as well as carriers with controlled composition and properties which satisfy the special requirements of various types of reactions [25–37]. The combustion temperature can reach up to 3000 °C (depending on the composition of the system) due to the exothermic reactions that occur within just a few minutes after the start of SHS synthesis. As a result of SHS, high-speed self-sustaining reactions, similar to autowave combustion, arise and develop, which lead to the formation of compositions with the required structure. They completely or partially exclude external energy supply and involve the use of internal heat, which is released as a result of chemical reactions. The control of temperature, degree of conversion, rate of the process, as well as composition of the target products is carried out by changing the rates of heat release. Such features contribute to the formation of important advantages over traditional methods of synthesis: a significantly shorter process time (only a few minutes), the synthesis of new materials, including catalysts, based on various elements of the Periodic Table, the simplicity of the equipment and used technological process, significantly lower consumption energy. The formation of defect structures with multiple deformations of the crystal lattice is caused by high rates of heating and cooling during the SHS period. The strong influence of defects on catalytic properties is a well-known fact. It has been found that many SHS catalysts are very active in various processes. As a result, SHS has become a widely studied discipline around the world.

Based on our previous research, the preparation of SHS catalysts for methane reforming with CO<sub>2</sub> has been very promising. Studies on catalysts synthesized by the new SHS method were carried out in [36,38–42]. In this work, we intend to study different compositions of catalysts for obtaining hydrogen-containing fuel mixtures. Systems based on Ni, Mg, Mn, and their mixtures were selected according to literature sources, and therefore, catalysts based on Ni/Mn were studied in this work in an effort at obtaining catalysts with increased activity and stability. Research on hydrogen concentration is currently underway, and the results will be presented in the future.

## 2. Materials and Methods

### 2.1. Preparation of SHS Catalysts

Ni-Mn-based oxides catalysts were produced on the base of the initial batch contained Mg, MgO, Mg (NO<sub>3</sub>)<sub>2</sub>, Al, Al<sub>2</sub>O<sub>3</sub>, NiO, and KMnO<sub>4</sub>. The initial batch composition for the 5 materials produced is presented in Table 1.

**Table 1.** Initial batch composition of the Ni-Mn series.

Name	Initial Batch Composition (wt%)				
	1 Ni-Mn	2 Ni-Mn	3 Ni-Mn	4 Ni-Mn	5 Ni-Mn
MgO	13.04	13.04	13.04	13.04	13.04
Al <sub>2</sub> O <sub>3</sub>	23.48	23.48	23.48	23.48	23.48
Mg (NO <sub>3</sub> ) <sub>2</sub>	30.44	30.44	30.44	30.44	30.44
KMnO <sub>4</sub>	21.04	16.70	13.04	10.52	4.34
NiO	0	4.34	8.00	10.52	16.70
Al	4.00	4.00	4.00	4.00	4.00
Mg	8.00	8.00	8.00	8.00	8.00

The required amount of metal nitrate, oxide, metal in the different ratios was mixed, formed in cylindrical molding forms of diameter 1 or 2 cm with the same length under a pressure of about 15 MPa, and placed in a furnace preheated at temperatures of 600–900 °C.

All samples were self-ignited, and their rate of speed of the combustion front was measured. After combustion in the SHS regime, the catalysts were immediately taken out of the furnace.

## 2.2. Characterisation

The synthesized catalysts were examined by X-ray diffraction (XRD) and scanning electron microscopy (SEM) with EDS analysis immediately after combustion. The specific surface area of the samples was also determined. The formation and identification of the phases were confirmed by powder X-ray powder diffraction in a SIEMENS SPELLMAN DF3 diffractometer using Cu Ka<sub>1</sub> with wavelength  $\lambda = 1.5406 \text{ \AA}$ . The step-scans were taken over the range of  $2\theta$  from 5 to 100° in steps of 0.03°/s. Crystal lattice plane parameters were calculated according to Bragg's law  $n\lambda = 2d\sin\theta$ . The SEM observations were carried out in a Quanta Inspect FEI scanning electron microscope, and the EDS patterns were carried out by an EDS analyzer on samples sputter-coated with gold with a coating thickness of 5–10 nm. The compressive strength of cylindrical samples with a diameter of 1 cm and a height of 2 cm was measured in a universal tester at an adjustable voltage of 100 kN and at a displacement rate of 100  $\mu\text{M}/\text{min}$ . The specific surface area of the SHS catalysts was determined by the Brunauer–Emmett–Teller (BET) method using nitrogen adsorption on either a Micrometrics ASAP 2010 instrument or a GAPP V-Sorb 2800 Analyzer. The sample was degassed at 200 °C in high vacuum before measurement.

## 2.3. Catalytic Activity Studies

The catalytic activity for CH<sub>4</sub> reforming with CO<sub>2</sub> was measured for crushed SHS catalyst with an average granule size of 3 mm. Catalysts were placed in a quartz tube and tested in a fixed bed flow reactor Carbolite STF 16/75 with controller Eurotherm 902 without prior reduction in a standard flow installation. The studies were carried out in the reaction mixture CH<sub>4</sub>: CO<sub>2</sub>: N<sub>2</sub> = 1:1:1 at a temperature of 700–900 °C and atmospheric pressure. The volumetric flow rate of the total flow was maintained at 860, 1720, 2580, and 3300 h<sup>-1</sup>. The effluents were analyzed in a gas chromatograph Dani GC 86.10 HT equipped with a 30 m steel column filled with HayeSep Q 80/100 Mesh, on which gases O<sub>2</sub>, N<sub>2</sub>, CO, CO<sub>2</sub>, H<sub>2</sub>, CH<sub>4</sub> were analyzed at 125 °C with a thermal conductivity detector (TCD) with high purity He as the gas carrier.

## 3. Results and Discussion

### 3.1. Characterisation of Catalysts

Figure 1 shows XRD patterns of SHS catalysts of the Ni-Mn series. The structure of the components of the catalysts as identified from the XRD spectra is the following: The spinel MgAl<sub>2</sub>O<sub>4</sub> appeared in cubic and orthorhombic structure, Al<sub>2</sub>O<sub>3</sub> also had orthorhombic structure. The rest of the spinels and oxides (Figure 1) had a cubic structure. Comparison

of the spinels' XRD peaks at different ratios of initial components showed that they had slightly shifted  $2\theta$ , which indicates a defective structure of SHS products.

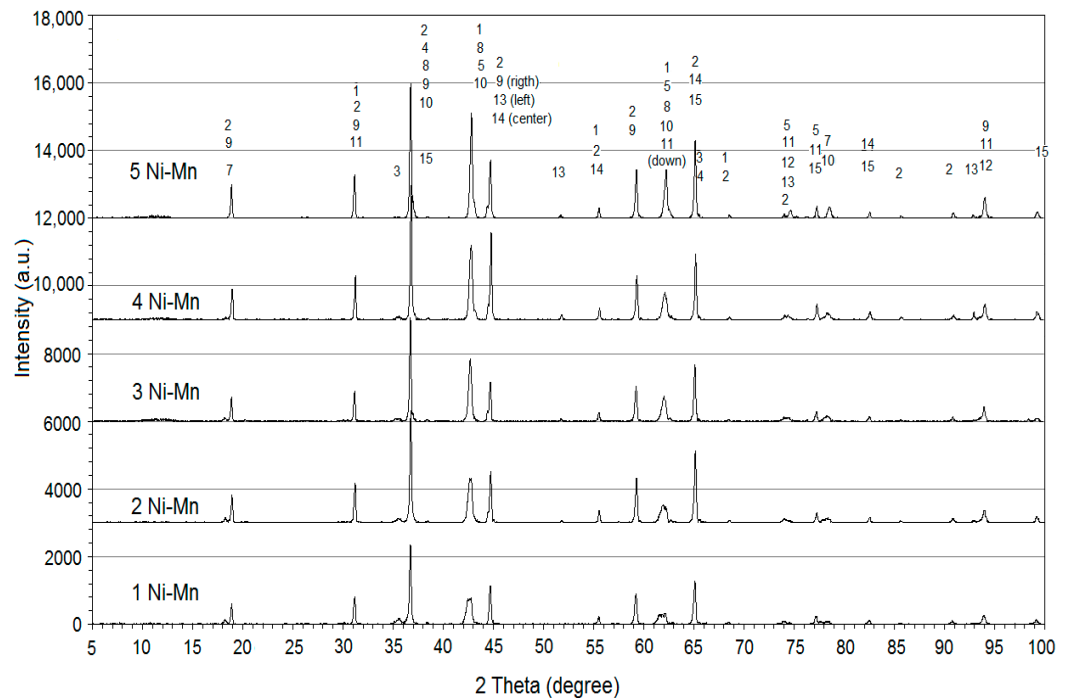
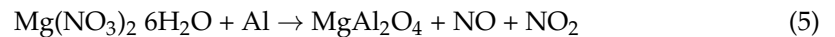
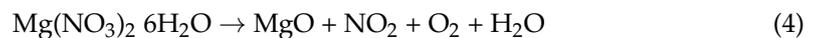


**Figure 1.** XRD patterns for Ni-Mn series of SHS catalysts. MgO—13.04%, Al<sub>2</sub>O<sub>3</sub>—23.48%, MgNO<sub>3</sub>—30.44%, KMnO<sub>4</sub>—4.34–21.04%, NiO—0–16.7%, Al—4%, Mg—8%. 1—MgAl<sub>2</sub>O<sub>4</sub> (orthorhombic), 2—MgAl<sub>2</sub>O<sub>4</sub> (cubic), 3—MnAl<sub>2</sub>O<sub>4</sub> (cubic), 4—MnAl<sub>2</sub>O<sub>4</sub>, 5—MgO (cubic), 6—Al<sub>2</sub>O<sub>3</sub>, 7—Mg<sub>6</sub>MnO<sub>8</sub>, 8—Mg<sub>0.9</sub>Mn<sub>0.1</sub>O, 9—NiAl<sub>2</sub>O<sub>4</sub>, 10—MgNiO<sub>2</sub>, 11—3MgO NiO, 12—MgO 3NiO.

The composition of catalysts' structures, as shown in Figure 1, can be explained by the following cascade reactions which take place during SHS process:



The presence of all the above products was also confirmed by EDS analysis on the SEM, for example, as shown in Figure 2 of Ni-Mn oxides-based SHS catalysts. The EDS spectra showed the existence of oxide compounds containing Ni, Mn, Mg, and Al, for

example, spinels and mixed oxides:  $\text{MgAl}_2\text{O}_4$ ,  $\text{MnAl}_2\text{O}_4$ ,  $\text{NiAl}_2\text{O}_4$ ,  $3\text{MgO} \cdot \text{NiO}$ , and  $\text{MgO} \cdot 3\text{NiO}$ . The origination of these compounds can be from sintering of oxides, but also by Mg ions replacement by Ni and Mn, first originated  $\text{MgAl}_2\text{O}_4$  spinel as shown in Figure 3. In Figure 3a, the EDS spectrum indicated  $\text{MgAl}_2\text{O}_4$ , where Mg was replaced by Ni and partially replaced by Mn. In the XRD spectra, these were presented as  $\text{MnAl}_2\text{O}_4$ ,  $\text{NiAl}_2\text{O}_4$ ,  $3\text{MgO} \cdot \text{NiO}$ , and  $\text{MgO} \cdot 3\text{NiO}$ . In Figure 3b, the EDS spectrum indicated  $\text{MgAl}_2\text{O}_4$ , where Mg was partially replaced by Ni and Mn. In the XRD spectra, these were presented as  $\text{MnAl}_2\text{O}_4$ ,  $\text{NiAl}_2\text{O}_4$ ,  $\text{MgAl}_2\text{O}_4$ ,  $3\text{MgO} \cdot \text{NiO}$ , and  $\text{MgO} \cdot 3\text{NiO}$ . In Figure 3c, the EDS spectrum also indicated  $\text{MgAl}_2\text{O}_4$ , where Mg was nearly completely replaced by Mn and the corresponding XRD spectra showed  $\text{MgAl}_2\text{O}_4$  and  $\text{MnAl}_2\text{O}_4$ . The degree of replacement of ions in the spinel structure depended on the concentration of Ni or Mn (Figure 4) in the initial SHS mixture and on the conditions of synthesis and cooling. These non-stoichiometric spinels originated during SHS due to the very high rate of synthesis heating and cooling which resulted in a high concentration of defects in SHS catalysts which were active centers of catalysis.

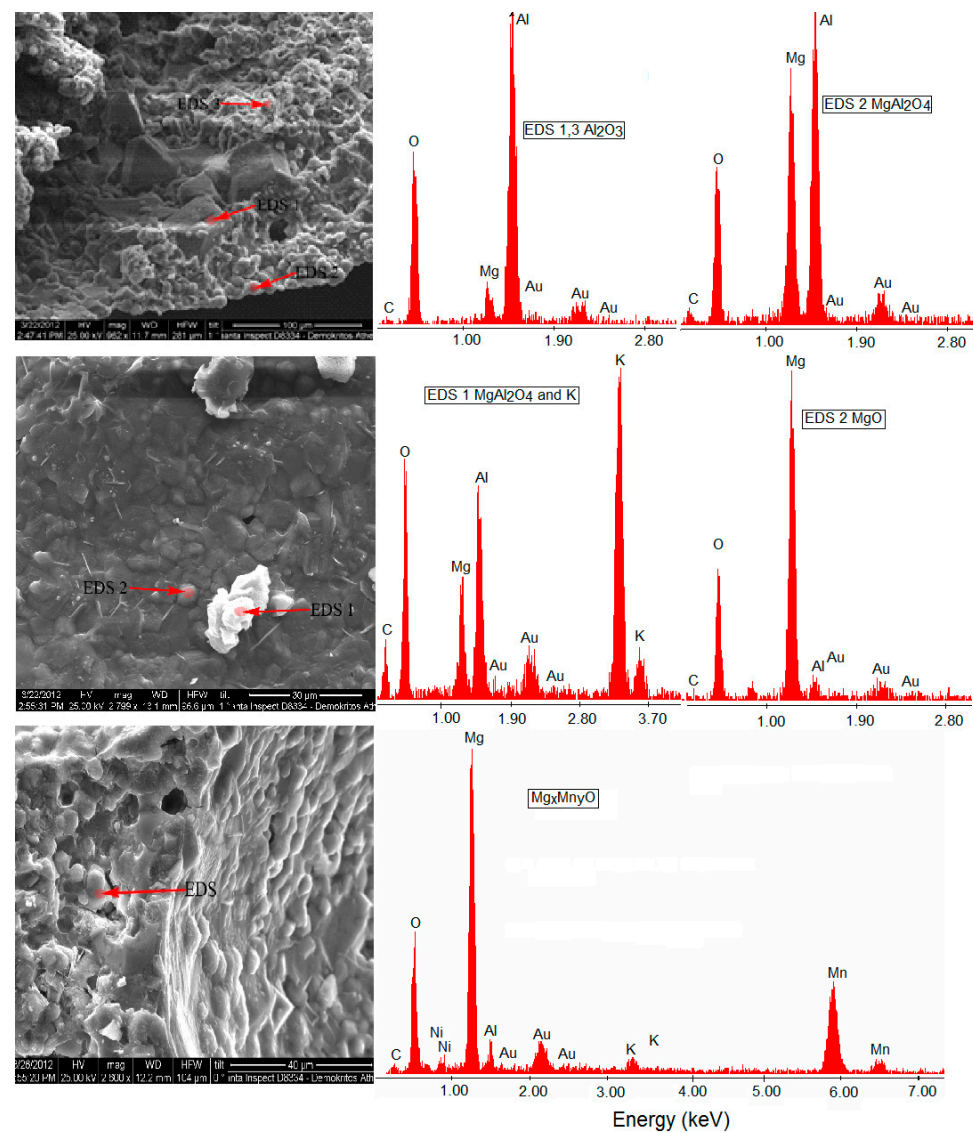


**Figure 2.** Initial batch: 13.04% MgO, 23.48%  $\text{Al}_2\text{O}_3$ , 30.44%  $\text{Mg}(\text{NO}_3)_2$ , 13.04%  $\text{KMnO}_4$ , 8% NiO, 4% Al, 8% Mg. Preheating temperature 600 °C.

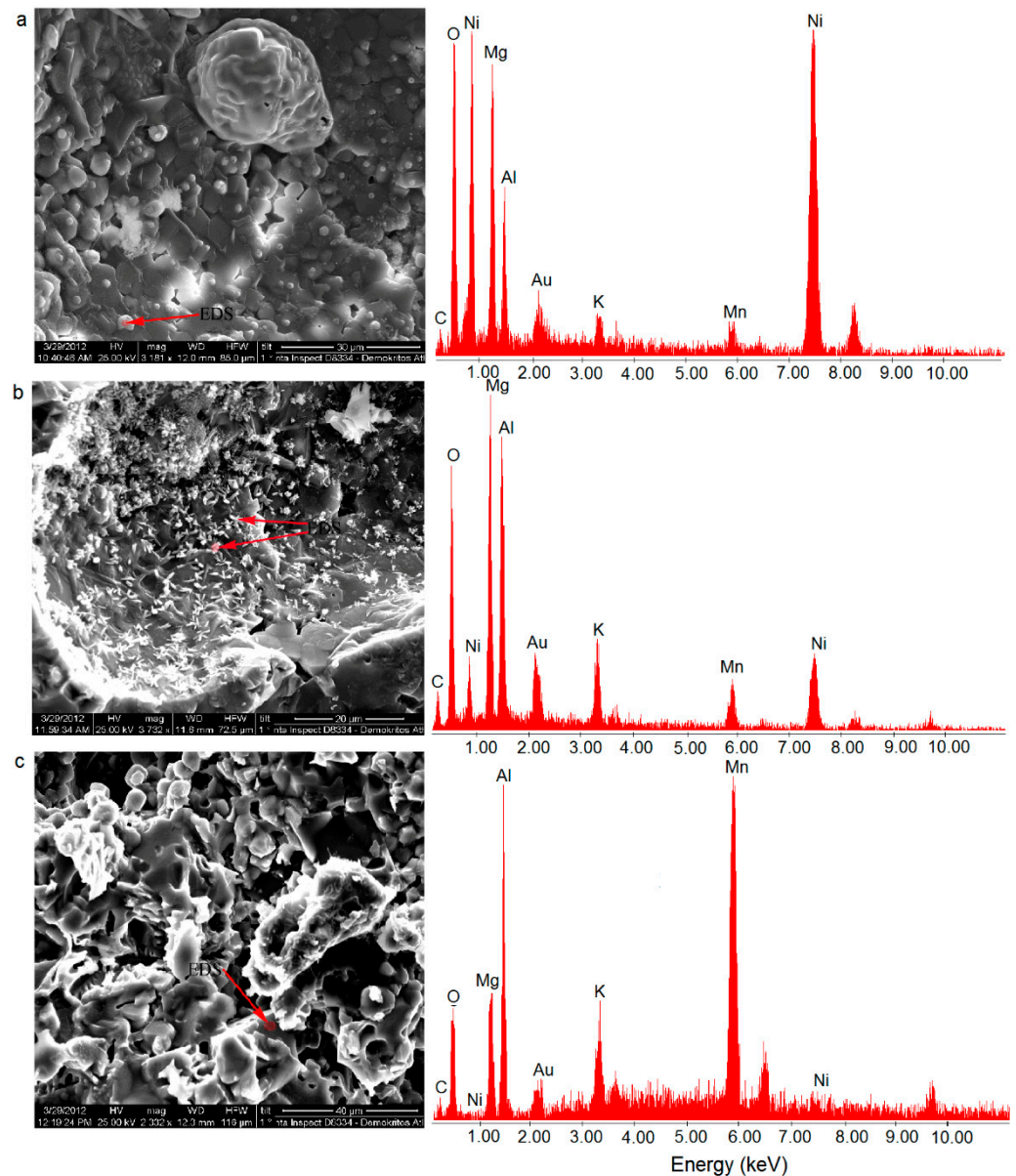


**Figure 3.** Initial batch: 13.04% MgO, 23.48% Al<sub>2</sub>O<sub>3</sub>, 30.44% Mg(NO<sub>3</sub>)<sub>2</sub>, 16.7% KMnO<sub>4</sub>, 4.34% NiO, 4% Al, 8% Mg. Preheating temperature 600 °C. (a) EDS spectrum of MgAl<sub>2</sub>O<sub>4</sub>, where Mg was replaced by Ni and partially replaced by Mn. MnAl<sub>2</sub>O<sub>4</sub>, NiAl<sub>2</sub>O<sub>4</sub>, 3MgO·NiO and MgO·3NiO present in XRD; (b) EDS spectrum of MgAl<sub>2</sub>O<sub>4</sub>, where Mg was partially replaced by Ni and Mn. MnAl<sub>2</sub>O<sub>4</sub>, NiAl<sub>2</sub>O<sub>4</sub>, MgAl<sub>2</sub>O<sub>4</sub>, 3MgO·NiO and MgO·3NiO present in XRD; (c) EDS spectrum of MgAl<sub>2</sub>O<sub>4</sub>, where Mg nearly completely replaced by Mn. MgAl<sub>2</sub>O<sub>4</sub> and MnAl<sub>2</sub>O<sub>4</sub> present in XRD.

Increasing spinel formation with increasing KMnO<sub>4</sub> in the initial batch is shown in Figure 4 and can be explained by increasing the input of the (9)–(13) reactions.

Increasing KMnO<sub>4</sub> in the initial batch did not seem to affect the parameters of Mg<sub>6</sub>MnO<sub>8</sub> crystal lattice because it was produced by the reaction of two oxides, as shown in Figure 5a:



In the case of MnAl<sub>2</sub>O<sub>4</sub>, increasing KMnO<sub>4</sub> led to a decrease in the crystal lattice parameters because MnAl<sub>2</sub>O<sub>4</sub> was produced mainly by Mg ion replacement by manganese in the MgAl<sub>2</sub>O<sub>4</sub> spinel. Since the ionic radius of Mn<sup>2+</sup> is 0.66 Å, and that of Mg<sup>2+</sup> is 0.8 Å, such substitutions lead to a decrease in the parameters of crystal lattice planes (Figure 5b).

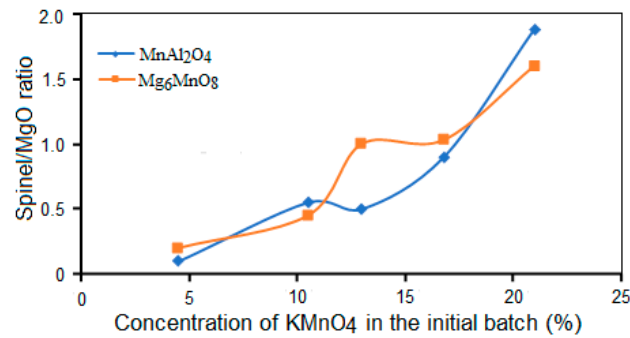


Figure 4. Influence of  $\text{KMnO}_4$  concentration in the initial batch on Mn spinels formation.

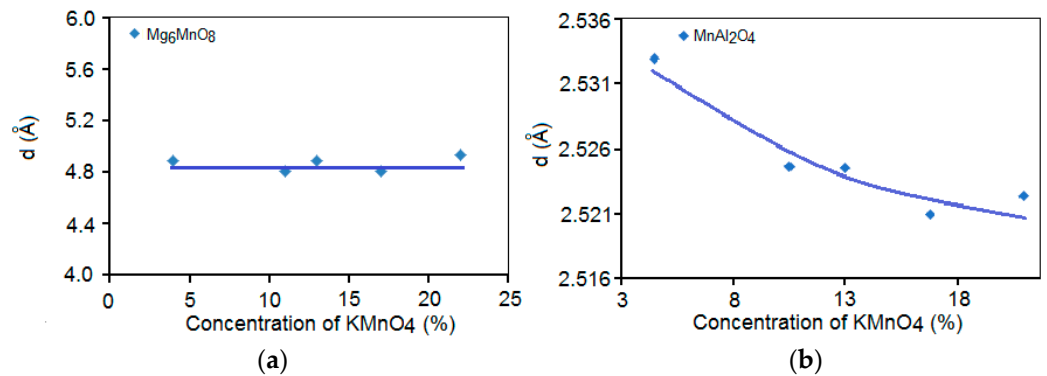


Figure 5. Influence of  $\text{KMnO}_4$  concentration in the initial batch: Al, Mg,  $\text{KMnO}_4$ , NiO, MgO,  $\text{Mg}(\text{NO}_3)_2$ ,  $\text{Al}_2\text{O}_3$  on the  $\text{Mg}_6\text{MnO}_8$  (a) and  $\text{MnAl}_2\text{O}_4$  (b) crystal lattice planes parameters in SHS catalysts.

Concentrations of  $\text{KMnO}_4$  and NiO in the initial batch as oxidizers influenced the velocity of SHS reactions (Figure 6a). Maximum velocity was found at 5% NiO and 13%  $\text{KMnO}_4$ , while it was moderate in the sample 2 Ni-Mn and 3 Ni-Mn, which were close to the stoichiometric ratio (Table 1). At these conditions, the highest combustion temperature was measured with sintering processes became more active, and as a consequence, the maximum strength of those catalysts (Figure 6b) was observed.

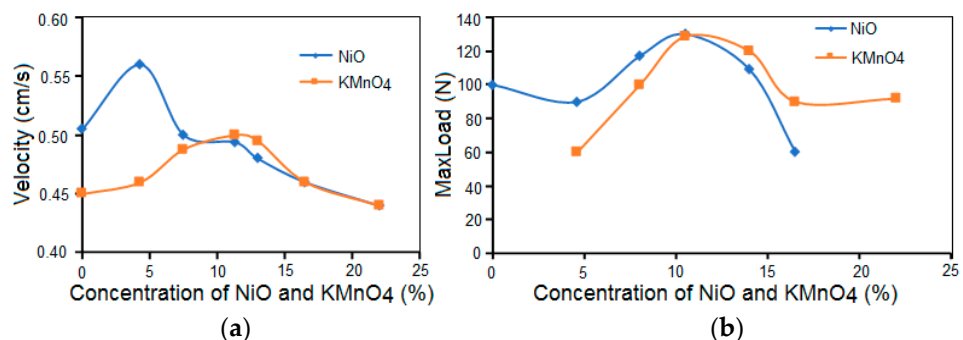
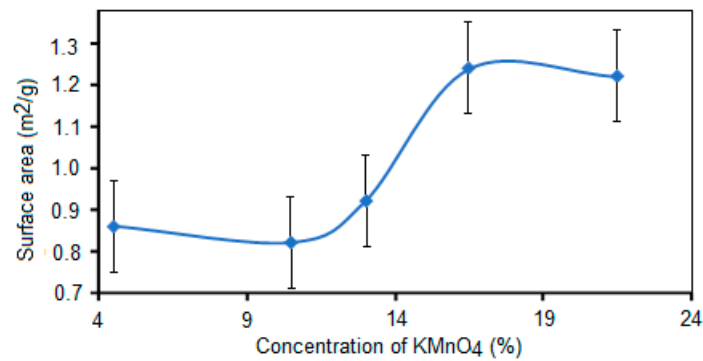


Figure 6. Influence of NiO and  $\text{KMnO}_4$  concentration in the initial batches of Ni-Mn series on the velocity of combustion during SHS (a) and SHS catalysts compressive strength (b).

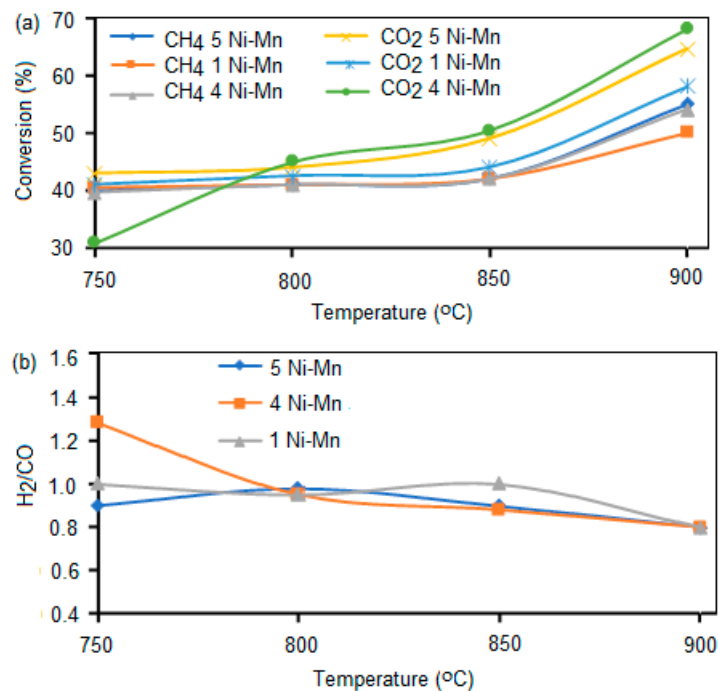
The specific surface area of the SHS catalysts is shown in Figure 7 and was very low ( $0.82\text{--}1.26\text{ m}^2/\text{g}$ ) because the combustion temperature for all compositions exceeded  $1200\text{ }^\circ\text{C}$ , and in those conditions, sintering processes take place. The increase in surface area with an increase in  $\text{KMnO}_4$  connected with the gas formation reaction  $\text{KMnO}_4 \rightarrow \text{KMnO}_2 + \text{O}_2$ , which increased porosity slightly.



**Figure 7.** Influence of KMnO<sub>4</sub> concentration in the initial batch on the SHS catalysts surface area.

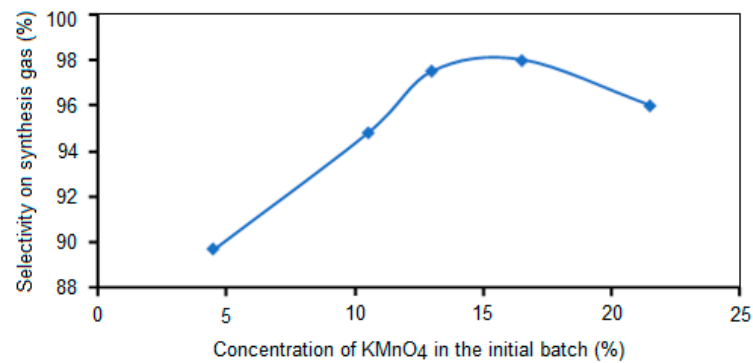
### 3.2. Catalytic Studies

The first experiments for conversion of CO<sub>2</sub> and CH<sub>4</sub> were carried out without catalysts and it was found that even at a temperature as high as 900 °C and low gas flow rate, the conversion of CH<sub>4</sub> was just 12% and that of CO<sub>2</sub>, just 11.4%. Thereafter, experiments were carried out in the presence of catalysts at different flow rates. Figure 8 shows the influence of reaction temperature and catalyst composition on the methane and carbon dioxide conversion and product H<sub>2</sub>/CO ratio using a flow rate of 860 h<sup>-1</sup>. An increase in the catalysis temperature for all studied Ni-Mn SHS catalysts led to an increase in CH<sub>4</sub> and CO<sub>2</sub> conversion, which is expected for catalysts since, at high temperatures, processes of adsorption and desorption are more intensive. However, increasing catalysis temperature did not affect products' H<sub>2</sub>/CO ratio, as shown in Figure 8.



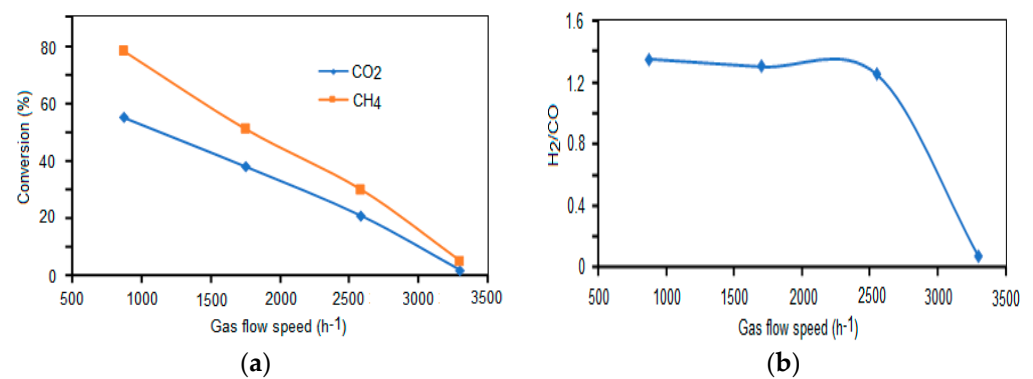
**Figure 8.** Influence of reaction temperature and catalyst composition on the methane and carbon dioxide conversion and product H<sub>2</sub>/CO ratio (flow rate 860 h<sup>-1</sup>).

Figure 9 shows that the selectivity of these catalysts was very high: between 72% and 98%. The high selectivity can also be verified by the small number of byproducts identified, including hydrocarbons (C<sub>2</sub>H<sub>6</sub>, C<sub>2</sub>H<sub>4</sub>, C) and H<sub>2</sub>O. Specifically, the catalyst made with 16.7% KMnO<sub>4</sub> in the initial SHS batch displayed the maximum selectivity at about 98%.



**Figure 9.** Selectivity of catalysts as a function of the concentration of KMnO<sub>4</sub> in the initial batch.

As expected, increasing the flow rate resulted in decreasing conversion. As can be seen in Figure 10a, conversion of CH<sub>4</sub> and CO<sub>2</sub> decreased, which indicated that the limiting stage, in this case, was a very low surface area (0.2–1.3 m<sup>2</sup>/g). Increasing the flow rate also led to a decrease in the dehydrogenation process and the ratio H<sub>2</sub>/CO decreased at a flow rate of more than 2500 h<sup>-1</sup> (Figure 10b). This is also shown by the increase in byproduct formation at those flow speeds. At a very high flow speed (3300 h<sup>-1</sup>), the product yield was low, and byproducts, such as H<sub>2</sub>O, C, and C<sub>2</sub>H<sub>6</sub>, were observed (Figure 11a). All in all, at high flow rates, the activity of those catalysts was low (Figure 11b).



**Figure 10.** Influence of gas flow speed on the CH<sub>4</sub> and CO<sub>2</sub> conversion (a) and H<sub>2</sub>/CO ratio (b) (catalyst 3 Mn-Ni, 900 °C).

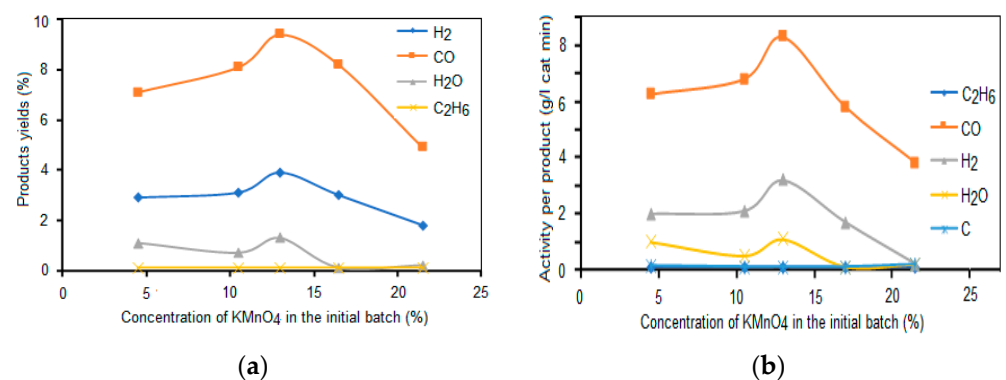


**Figure 11.** Influence of KMnO<sub>4</sub> concentration in the initial batch on the products yields (a) and catalytic activity per product (b).

In Figure 11a,b, it can be seen that the catalysts with 13% KMnO<sub>4</sub> in the initial batch displayed high performance regarding the yield of the products and the activity per product.

The influence of the catalyst preparation method was investigated on 5 Ni-Mn catalysts. Figure 12 shows data on conversion, selectivity, and H<sub>2</sub>/CO ratio depending on temperature on catalysts prepared by the SHS method compared with the traditional incipient wetness impregnation method. It was shown that the conversion of the initial materials, selectivity, and the ratio of reaction products were higher for SHS samples. Taking into account that the SHS method leads to the formation of catalytically active composites upon initiating heating for several minutes in comparison with many hours of heat treatment by the impregnation method, the production of synthesis gas has distinct advantages and is more profitable under the above-described conditions.

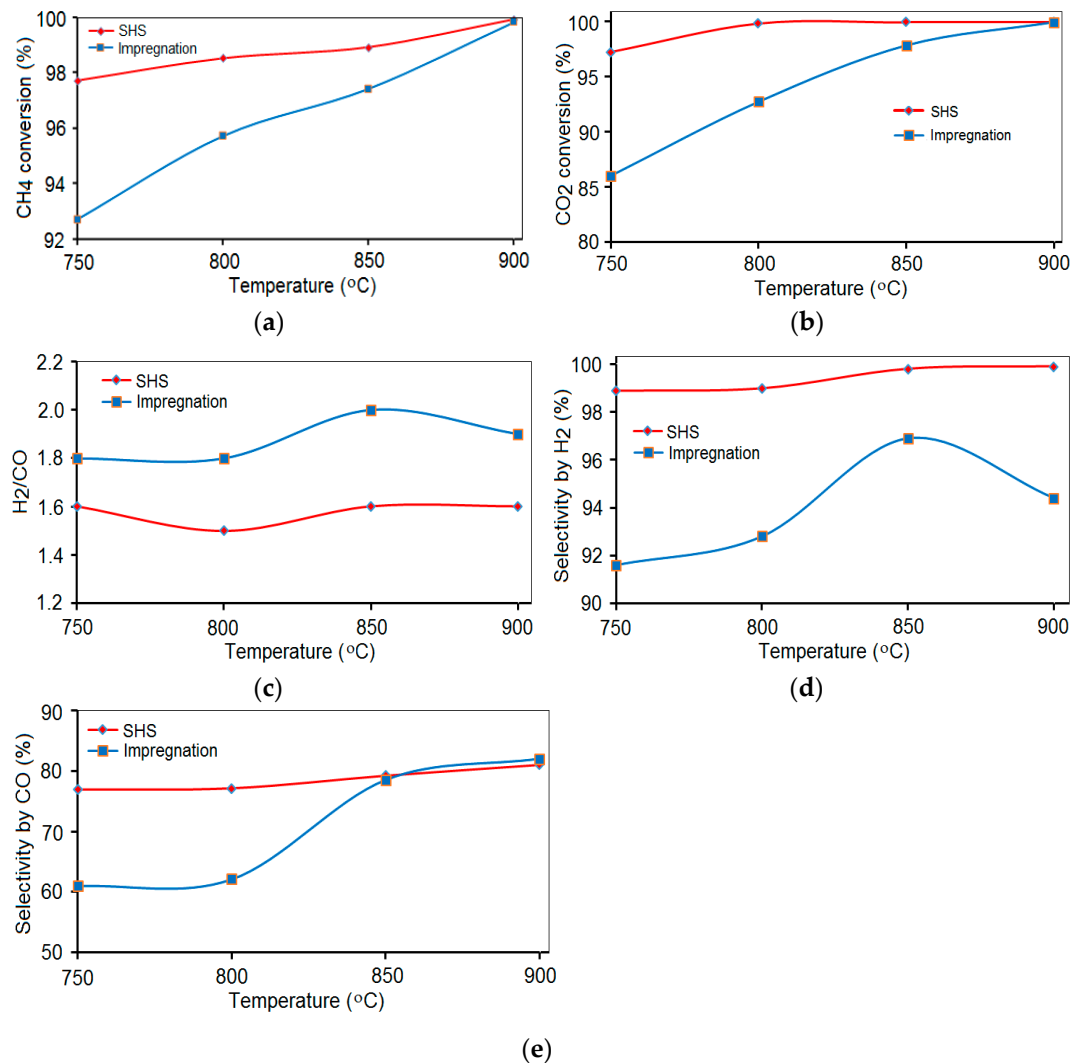


**Figure 12.** Influence of reaction temperature and method of catalyst preparation on the CH<sub>4</sub> (a) and CO<sub>2</sub> (b) conversion, H<sub>2</sub>/CO ratio (c), and selectivity by H<sub>2</sub> (d) and CO (e).

#### 4. Conclusions

This paper presents a study on the production and the properties of materials with catalytic activity for carbon dioxide reforming methane, produced using the self-propagating high-temperature synthesis (SHS) method. The study was focused on the systems Ni-Mn-Mg-Al-O and Mn-Mg-Al-O, which were found to be active systems for the CO<sub>2</sub>, dry CH<sub>4</sub> reforming process. In the Ni-Mn series tested, the max load under compression was found to increase with the increasing concentration of KMnO<sub>4</sub> in the initial batch because there was an increase in the total amount of spinel. The surface area of the catalysts was found to be very low due to the high temperature, which resulted in the sintering of the material during

SHS. It was also found that non-stoichiometric spinels were formed preferentially during SHS due to the high rate of synthesis heating and cooling, which resulted in an extensively defective structure in these SHS catalysts, which acted as active centers of catalysis and were the reason for their measured high catalytic activity.

The Ni-Mn catalysts produced displayed good performance in the conversion of the reactant gases and in their activity. Additionally, the SHS catalysts had very high selectivity that reached 98%. The catalysts of the Ni-Mn series at a low flow rate showed the best catalytic performance, which was expected because the Ni-Mn catalysts have a low surface area. Further increasing the specific surface area is necessary to increase the activity of these catalysts at a high flow rate. This can be done by using the solution combustion synthesis method (SCS). The production of CO and hydrogen was high and the yield of the products was up to 10%. The catalyst with the most promising catalytic performance had the following composition in the initial batch: MgO: 13.04%, Al<sub>2</sub>O<sub>3</sub>: 23.48%, MgNO<sub>3</sub>: 30.44%, KMnO<sub>4</sub>: 13.04%, NiO: 16.7%, Al: 4.0%, Mg: 8.0%.

In general, SHS is a very rapid and low-cost method for catalyst production, and promising results were received for active catalysts for the carbon dioxide reforming of methane process.

**Author Contributions:** Conceptualization, G.X. and S.A.T.; methodology, S.V.; software, M.Z.; validation, G.X. and G.V.; formal analysis, M.Z.; investigation, K.K.; resources, T.S.B.; data curation, S.V.; writing—original draft preparation, G.X.; writing—review and editing, G.V.; visualization, T.S.B.; supervision, S.A.T.; project administration, T.S.B.; funding acquisition, S.A.T. All authors have read and agreed to the published version of the manuscript.

**Funding:** This research was funded by the Science Committee of the Ministry of Education and Science of the Republic of Kazakhstan, grant number AP08855562.

**Institutional Review Board Statement:** Not applicable.

**Informed Consent Statement:** Not applicable.

**Data Availability Statement:** The data presented in this study are available upon request from the corresponding author.

**Acknowledgments:** The authors are especially grateful to the Brodskii A.R. and Komashko L.V. from the laboratory of physical and chemical research methods.

**Conflicts of Interest:** The authors declare no conflict of interest. The funders had no role in the design of the study; in the collection, analyses, or interpretation of data; in the writing of the manuscript, or in the decision to publish the results.

## References

1. IEA World Energy Outlook. 2010. Available online: <https://webstore.iea.org/world-energy-outlook-2010> (accessed on 10 September 2019).
2. The Intergovernmental Panel on Climate Change. Available online: <https://www.ipcc.ch/> (accessed on 11 March 2017).
3. IPCC Review. Available online: [Chrome-extension://efaidnbnmnibpcjpcglclefindmkaj/viewer.html?pdfurl=https%3A%2F%2Fwwwf.ru%2Fupload%2Fiblock%2F790%2Fipcc\\_review.pdf&clen=3866352&chunk=true](https://chrome-extension://efaidnbnmnibpcjpcglclefindmkaj/viewer.html?pdfurl=https%3A%2F%2Fwwwf.ru%2Fupload%2Fiblock%2F790%2Fipcc_review.pdf&clen=3866352&chunk=true) (accessed on 25 January 2021).
4. United States Environmental Protection Agency. Available online: <https://www.epa.gov/gmi/importance-methane> (accessed on 30 June 2021).
5. Estifae, P.; Haghighi, M.; Babaluo, A.A.; Rahemi, N.; Jafari, M.F. The beneficial use of non-thermal plasma in synthesis of Ni/Al<sub>2</sub>O<sub>3</sub>-MgO nano-catalyst used in hydrogen production from reforming of CH<sub>4</sub>/CO<sub>2</sub> greenhouse gases. *J. Power Sources* **2014**, *257*, 364–373. [CrossRef]
6. Movasati, A.; Alavi, S.M.; Mazloom, G. Dry reforming of methane over CeO<sub>2</sub>-ZnAl<sub>2</sub>O<sub>4</sub> supported Ni and Ni-Co nano-catalysts. *Fuel* **2019**, *236*, 1254–1262. [CrossRef]
7. Adans, Y.F.; Ballarini, A.D.; Martins, A.R.; Coelho, R.E.; Carvalho, L.S. Performance of nickel supported on  $\gamma$ -alumina obtained by aluminum recycling for methane dry reforming. *Catal. Lett.* **2017**, *147*, 2057–2066. [CrossRef]
8. Ali, S.; Khader, M.M.; Almarri, M.J.; Abdelmoneim, A.G. Ni-based nano-catalysts for the dry reforming of methane. *Catal. Today* **2020**, *343*, 26–37. [CrossRef]
9. Larimi, S.; Alavi, S.M. Partial oxidation of methane over Ni/CeZrO<sub>2</sub> mixed oxide solid solution catalysts. *Int. J. Chem. Eng. Appl.* **2012**, *3*, 6–9. [CrossRef]

10. Soloviev, S.O.; Kapran, A.Y.; Orlyk, S.N.; Gubareni, E.V. Carbon dioxide reforming of methane on monolithic Ni/Al<sub>2</sub>O<sub>3</sub>-based catalysts. *J. Nat. Gas Chem.* **2011**, *20*, 184–190. [[CrossRef](#)]
11. Fidalgo, B.; Arenillas, A.; Menendez, J.A. Synergetic effect of a mixture of activated carbon + Ni/Al<sub>2</sub>O<sub>3</sub> used as catalysts for the CO<sub>2</sub> reforming of CH<sub>4</sub>. *Appl. Catal. A Gen.* **2010**, *390*, 78–83. [[CrossRef](#)]
12. Moniri, A.; Alavi, S.M.; Rezaei, M. Syngas production by combined carbon dioxide reforming and partial oxidation of methane over Ni/ $\alpha$ -Al<sub>2</sub>O<sub>3</sub> catalysts. *J. Nat. Gas Chem.* **2010**, *19*, 638–641. [[CrossRef](#)]
13. Ni, J.; Chen, L.; Lin, J.; Kawi, S. Carbon deposition on borated alumina supported nano-sized Ni catalysts for dry reforming of CH<sub>4</sub>. *Nano Energy* **2012**, *1*, 674–686. [[CrossRef](#)]
14. Meshkani, F.; Rezaei, M. Nanocrystalline MgO supported nickel-based bimetallic catalysts for carbon dioxide reforming of methane. *Int. J. Hydrogen Energy* **2010**, *35*, 10295–10301. [[CrossRef](#)]
15. Wang, N.; Chu, W.; Zhang, T.; Zhao, X.S. Manganese promoting effects on the Co–Ce–Zr–O<sub>x</sub> nano catalysts for methane dry reforming with carbon dioxide to hydrogen and carbon monoxide. *Chem. Eng. J.* **2011**, *170*, 457–463. [[CrossRef](#)]
16. Horváth, É.; Baán, K.; Varga, E.; Oszkó, A.; Vágó, Á.; Törő, M.; Erdőhelyi, A. Dry reforming of CH<sub>4</sub> on Co/Al<sub>2</sub>O<sub>3</sub> catalysts reduced at different temperatures. *Catal. Today* **2017**, *281*, 233–240. [[CrossRef](#)]
17. Özkara-Aydinoğlu, S.; Aksoylu, A.E. Carbon dioxide reforming of methane over Co-X/ZrO<sub>2</sub> catalysts (X=La, Ce, Mn, Mg, K). *Catal. Commun.* **2010**, *11*, 1165–1170. [[CrossRef](#)]
18. Aramouni, N.A.K.; Zeaiter, J.; Kwapinski, W.; Leahy, J.J.; Ahmad, M.N. Eclectic trimetallic Ni-Co-Ru catalyst for the dry reforming of methane. *Int. J. Hydrog. Energy* **2020**, *45*, 17153–17163. [[CrossRef](#)]
19. Turap, Y.; Wang, L.; Fu, T.; Wu, Y.; Wang, Y.; Wang, W. Co–Ni alloy supported on CeO<sub>2</sub> as a bimetallic catalyst for dry reforming of methane. *Int. J. Hydrog. Energy* **2020**, *45*, 6538–6548. [[CrossRef](#)]
20. Siang, T.J.; Singh, S.; Omoregbe, O.; Bach, L.G.; Phuc, N.H.H.; Vo, D.V.N. Hydrogen production from CH<sub>4</sub> dry reforming over bimetallic Ni-Co/Al<sub>2</sub>O<sub>3</sub> catalyst. *J. Energy Inst.* **2018**, *91*, 683–694. [[CrossRef](#)]
21. Jalali, R.; Rezaei, M.; Nematollahi, B.; Baghalha, M. Preparation of Ni/MeAl<sub>2</sub>O<sub>4</sub>-MgAl<sub>2</sub>O<sub>4</sub> (Me=Fe, Co, Ni, Cu, Zn, Mg) nanocatalysts for the syngas production via combined dry reforming and partial oxidation of methane. *Renew. Energy* **2020**, *149*, 1053–1067. [[CrossRef](#)]
22. Wu, H.; Liu, H.; Yang, W.; He, D. Synergetic effect of Ni and Co in Ni–Co/SBA-15-CD catalysts and their catalytic performance in carbon dioxide reforming of methane to syngas. *Catal. Sci. Technol.* **2016**, *6*, 5631–5646. [[CrossRef](#)]
23. Kim, W.Y.; Jang, J.S.; Ra, E.C.; Kim, K.Y.; Kim, E.H.; Lee, J.S. Reduced perovskite LaNiO<sub>3</sub> catalysts modified with Co and Mn for low coke formation in dry reforming of methane. *Appl. Catal. A Gen.* **2019**, *575*, 198–203. [[CrossRef](#)]
24. Merzhanov, A.G. Worldwide evolution and present status of SHS as a branch of modern R&D. *Int. J. Self-Propag. High-Temp. Synth.* **1997**, *6*, 119–163.
25. Xanthopoulou, G. Catalytic properties of the SHS products: Review. *Adv. Sci. Technol.* **2010**, *63*, 287–296. [[CrossRef](#)]
26. Pramono, A.; Kommel, L.; Kollo, L.; Veinthal, R. The aluminum based composite produced by self propagating high temperature synthesis. *Mater. Sci. (Medžg.)* **2016**, *22*, 41–43. [[CrossRef](#)]
27. Varma, A.; Mukasyan, A.S.; Rogachev, A.S.; Manukyan, K.V. Solution combustion synthesis of nanoscale materials. *Chem. Rev.* **2016**, *116*, 14493–14586. [[CrossRef](#)] [[PubMed](#)]
28. Xanthopoulou, G.; Thoda, O.; Roslyakov, S.; Steinman, A.; Kovalev, D.; Levashov, E.; Vekinis, G.; Sytschev, A.; Chroneos, A. Solution combustion synthesis of nano-catalysts with a hierarchical structure. *J. Catal.* **2018**, *364*, 112–124. [[CrossRef](#)]
29. Khaliullin, S.M.; Zhuravlev, V.D.; Bamburov, V.G. Solution-combustion synthesis of oxide nanoparticles from nitrate solutions containing glycine and urea: Thermodynamic aspects. *Int. J. Self-Propag. High-Temp. Synth.* **2016**, *25*, 139–148. [[CrossRef](#)]
30. Thoda, O.; Xanthopoulou, G.; Vekinis, G.; Chroneos, A. The effect of the precursor solution's pretreatment on the properties and microstructure of the SCS final nanomaterials. *Appl. Sci.* **2019**, *9*, 1200. [[CrossRef](#)]
31. Xanthopoulou, G.G.; Vekinis, G.A. Catalytic pyrolysis of naphtha on the SHS catalysts. *Eurasian Chem.-Technol. J.* **2010**, *12*, 17–21. [[CrossRef](#)]
32. Bera, P. Solution combustion synthesis as a novel route to preparation of catalysts. *Int. J. Self-Propag. High-Temp. Synth.* **2019**, *28*, 77–109. [[CrossRef](#)]
33. Xanthopoulou, G.; Thoda, O.; Boukos, N.; Krishnamurthy, S.; Dey, A.; Roslyakov, S.; Vekinis, G.; Chroneos, A.; Levashov, E. Effects of precursor concentration in solvent and nanomaterials room temperature aging on the growth morphology and surface characteristics of Ni–NiO nanocatalysts produced by dendrites combustion during SCS. *Appl. Sci.* **2019**, *9*, 4925. [[CrossRef](#)]
34. Xanthopoulou, G. Some advanced applications of SHS: An Overview. *Int. J. Self-Propag. High-Temp. Synth.* **2011**, *20*, 269–272. [[CrossRef](#)]
35. Qiu, B.; Wang, W.; Yang, X. Computational design of SCS nickel pincer complexes for the asymmetric transfer hydrogenation of 1-acetonaphthone. *Catalysts* **2019**, *9*, 101. [[CrossRef](#)]
36. Tungatarova, S.; Xanthopoulou, G.; Karanasios, K.; Baizhumanova, T.; Zhumabek, M.; Kaumenova, G. New composite materials prepared by solution combustion synthesis for catalytic reforming of methane. *Chem. Eng. Trans.* **2017**, *61*, 1921–1926. [[CrossRef](#)]
37. Singsarothai, S.; Khanghamano, M.; Rachphet, V.; Niyomwas, S. Influence of CaO<sub>2</sub> additives on the properties of Fe-WB-based composite lining deposited by centrifugal SHS on the inner surface of steel pipe. *Int. J. Self-Propag. High-Temp. Synth.* **2016**, *25*, 181–185. [[CrossRef](#)]

38. Pino, L.; Vita, A.; Laganà, M.; Recupero, V. Hydrogen from biogas: Catalytic tri-reforming process with Ni/LaCeO mixed oxides. *Appl. Catal. B Environ.* **2014**, *148–149*, 91–105. [[CrossRef](#)]
39. Postole, G.; Nguyen, T.-S.; Aouine, M.; Gélín, P.; Cardenas, L.; Piccolo, L. Efficient hydrogen production from methane over iridium-doped ceria catalysts synthesized by solution combustion. *Appl. Catal. B Environ.* **2015**, *166–167*, 580–591. [[CrossRef](#)]
40. Vita, A.; Italiano, C.; Fabiano, C.; Laganà, M.; Pino, L. Influence of Ce-precursor and fuel on structure and catalytic activity of combustion synthesized Ni/CeO<sub>2</sub> catalysts for biogas oxidative steam reforming. *Mater. Chem. Phys.* **2015**, *163*, 337–347. [[CrossRef](#)]
41. Xanthopoulou, G.; Karanasios, K.; Tungatarova, S.; Baizhumanova, T.; Zhumabek, M.; Kaumenova, G.; Massalimova, B.; Shorayeva, K. Catalytic methane reforming into synthesis-gas over developed composite materials prepared by combustion synthesis. *React. Kinet. Mech. Catal.* **2019**, *126*, 645–661. [[CrossRef](#)]
42. Karanasios, K.; Xanthopoulou, G.; Vekinis, G.; Zoumpoulakis, L. Co-Al-O catalysts produced by SHS method for CO<sub>2</sub> reforming of CH<sub>4</sub>. *Int. J. Self-Prop. High-Temp. Synth.* **2014**, *23*, 221–229.